

The Energy Level Alignment at the Buffer/Cu(In,Ga)Se₂ Thin-Film Solar Cell Interface for CdS and GaO_x

Donald Valenta,* Hasan Arif Yetkin, Tim Kodalle, Jakob Bombsch, Raul Garcia-Diez, Claudia Hartmann, Shigenori Ueda, Roberto Félix, Johannes Frisch, Lucas Bodenstein-Dresler, Regan G. Wilks,* Christian A. Kaufmann, and Marcus Bär*

Sputter-deposited GaO_x (i.e., oxygen-deficient gallium oxide) films are evaluated as a potential replacement for the standard CdS buffer layers in Cu(In,Ga)Se₂ (CIGSe) based thin-film photovoltaics. The energy level alignment at the GaO_x/CIGSe and CdS/CIGSe interfaces are compared by means of direct and inverse photoemission. For the GaO_x/CIGSe a (0.04 ± 0.07) eV (i.e., a small spike-like) conduction band offset (CBO) and a (-3.21 ± 0.19) eV (i.e., a large cliff-like) valence band offset (VBO) are found, which suggests a nearly ideal charge-selective contact. The derived GaO_x band gap of (4.80 ± 0.25) eV confirms its utility as a highly transparent buffer layer. However, the GaO_x (with x derived to be 1.1 ± 0.1) exhibits considerable (presumably) defect-related occupied states above the valence band maximum. It is proposed that these states may increase charge carrier recombination and decrease open circuit voltage in respective devices; also explaining why solar cells with standard CdS buffer outperform devices with GaO_x buffer, despite less ideal electronic interface properties (CBO: (-0.18 ± 0.07) eV, VBO: (-0.98 ± 0.15) eV) and the smaller CdS band gap of (2.35 ± 0.22) eV.

1. Introduction

Thin-film solar cells based on Cu(In,Ga)Se₂ (CIGSe) chalcopyrite light absorbers are a stable, low band gap bottom device technology for tandem solar cells. They are potentially flexible and lightweight and low material and energy consumption promises lower production costs. CIGSe devices can reach power conversion efficiencies exceeding >23%.^[1,2] For these high efficiencies, cadmium sulfide (CdS) is commonly employed as a buffer layer between the CIGSe absorber and the emitter. The use of a heavy metal, Cd, and parasitic absorption due to the short-wavelength range are strong motivations for replacing it with a nontoxic, more transparent alternative buffer. To be considered a viable alternative to CdS in CIGSe-based solar cells, certain requirements must

D. Valenta, J. Bombsch, R. Garcia-Diez, C. Hartmann, R. Félix, J. Frisch, L. Bodenstein-Dresler, R. G. Wilks, M. Bär
Interface Design
Helmholtz-Zentrum Berlin für Materialien und Energie GmbH (HZB)
Berlin Germany
E-mail: donald.valenta@helmholtz-berlin.de;
regan.wilks@helmholtz-berlin.de; marcus.baer@helmholtz-berlin.de
H. A. Yetkin, T. Kodalle, C. A. Kaufmann
PVcomB
HZB
Berlin Germany
S. Ueda
Synchrotron X-ray Station at SPring-8
National Institute for Materials Science (NIMS)
Kouto, Sayo, Hyogo Japan

S. Ueda
Research Center for Electronic and Optical Materials
NIMS
Tsukuba, Ibaraki Japan
R. Félix, J. Frisch, R. G. Wilks, M. Bär
Energy Materials In-Situ Laboratory Berlin (EMIL)
HZB
Berlin Germany
M. Bär
Helmholtz-Institute Erlangen-Nürnberg for Renewable Energy (HIERN)
Berlin Germany
M. Bär
Department of Chemistry and Pharmacy
Friedrich-Alexander-Universität Erlangen-Nürnberg (FAU)
Erlangen Germany

 The ORCID identification number(s) for the author(s) of this article can be found under <https://doi.org/10.1002/admi.202301110>

© 2024 The Authors. Advanced Materials Interfaces published by Wiley-VCH GmbH. This is an open access article under the terms of the [Creative Commons Attribution](#) License, which permits use, distribution and reproduction in any medium, provided the original work is properly cited.

DOI: 10.1002/admi.202301110

be fulfilled.^[3] The conduction band offset (CBO) is one of the most crucial parameters for unimpeded electron transport across the buffer/absorber.^[4] An aligned conduction band (i.e., a CBO of zero) is ideal for electron transport, however, theoretical analysis^[5–7] shows that high performance can also be obtained with a positive CBO of up to +0.2 to +0.4 eV and with a negative CBO of up to –0.1 to –0.4 eV depending on whether or not a Cu-poor CIGSe surface layer (often called OVC—ordered vacancy compound)^[8,9] is present and how in the underlying models the offset is distributed between the CdS/OVC and the OVC/CIGSe interfaces. For CdS/chalcopyrite stacks resulting in high-efficiency solar cells, aligned^[10,11] or slightly positive^[11,12] CBO values have, indeed, been reported in the past.

Gallium oxide is a wide band gap semiconductor prominent for field effect passivation^[13,14] with minimal related environmental and health concerns and thus is a possible CdS buffer layer alternative candidate material. It displays n-type conductivity when O-deficient compared to its Ga₂O₃ stoichiometry (we will refer to such material as GaO_x below).^[3,15–18] This n-type conductivity is attributed to oxygen vacancy-derived defect states; consequently, the conductivity of GaO_x films is generally connected to an oxygen-deficient environment during the preparation process,^[9,11] which may open a convenient route for deliberately tuning the electronic structure of GaO_x when applied as buffer layer in CIGSe devices. GaO_x films may also fulfill another highly desirable requirement, namely producing an interface that is less prone to temperature-induced interdiffusion (compared to layer stacks with CdS as interface partners). This is a crucial requirement to benefit from high-temperature deposition of the transparent conductive oxide (used as front contact) or for the application of CIGSe cells in tandem or multijunction devices to avoid negative effects of subsequent high-temperature process stages (e.g., during the deposition of the top cell).^[18]

In this work, we compare the electronic structure (and here specifically the energy level alignment at the interface) of the standard buffer/absorber interface CdS/CIGSe with that of the potential alternative GaO_x/CIGSe. In order to do so, we combined several photoelectron spectroscopy techniques such as synchrotron-based hard X-ray photoelectron spectroscopy (HAXPES), lab-based X-ray photoelectron spectroscopy (XPS), lab-based ultraviolet photoelectron spectroscopy (UPS) and inverse photoelectron spectroscopy (IPES) to thoroughly study and directly determine the electronic structure at the buffer/absorber interfaces. The derived energy level alignment will provide a detailed insight into the charge carrier transport mechanism across the buffer/absorber interface and how it may affect device efficiency.

2. Experimental Section

2.1. Sample Preparation

In this study, buffer/CIGSe samples were made at the Competence Centre for Photovoltaics Berlin (PVcomB) at HZB employing their standard deposition process.^[19] On a cleaned 50 × 50 × 2 mm³ soda-lime glass (SLG) substrate, the molybdenum back contact of 800 nm thickness was deposited by DC sputtering, followed by the 2.1-μm-thick CIGSe thin-film absorber prepared by a three-stage physical vapor deposition (PVD) pro-

cess. To complete the buffer/CIGSe/Mo/SLG stack, buffer layers of CdS or GaO_x were deposited (a thorough characterization of the physical properties of similarly prepared buffer layers and related devices has previously been reported^[19]). For CdS deposition the CIGSe was first rinsed in a 2.5% aqueous ammonia solution, followed by chemical bath deposition (CBD) using anhydrous cadmium acetate (Cd(CH₃COOH)₂) and thiourea (S=C(NH₂)₂) in an aqueous ammonia-containing solution. To obtain a nominal layer thickness of 50 nm, the CIGSe/Mo/SLG stack was immersed into 1800 mL CBD solution for 16 min during which the temperature of the CBD solution increased from 25 to ≈50 °C. Thinner layers were produced by interrupting the CBD earlier; a 10 nm nominal thickness was obtained after a CdS CBD of 4 min and 36 s. The 5- and 50-nm-thick GaO_x buffer layers were deposited via radio frequency (RF) magnetron sputtering using a 5 N stoichiometric Ga₂O₃ target. Deposition was carried out with 70 W power in an Ar₂ atmosphere with a sputtering pressure of 5 μbar without additional oxygen. During the sputtering process, the substrate was not externally heated. After the deposition processes, in both cases, the buffer/absorber samples were vacuum-sealed to minimize air exposure and surface contamination. Solar cells prepared using identical processes resulted in efficiencies of 13.0% for devices with GaO_x buffer and 16.2% for CdS buffered cells.^[18]

2.2. Photoelectron Spectroscopy

HAXPES measurements were performed using an excitation energy of linearly polarized 5.95 keV X-rays (referred to as 6 keV in this manuscript) at BL15XU of the SPring-8 electron storage ring,^[20] equipped with a hemispherical electron analyzer (VG Scienta R4000) oriented perpendicular to the X-ray propagation access and with the analyzer axis and X-ray polarization vector aligned. Using the high-resolution Si 333 channel-cut monochromator and an electron analyzer pass energy of 200 eV, a total energy resolution of 0.25 eV was achieved for all HAXPES measurements. Calibration of the binding energy was done by referencing the Au 4f_{7/2} peak to 84.00 eV. The base pressure of the analysis chamber during measurements was <6 × 10^{–9} mbar. The take-off-angle of photoelectrons was set to ≈88° with respect to the sample surface for all measurements.

Laboratory-based XPS and UPS measurements were performed in the Energy Materials In Situ Laboratory Berlin (EMIL) at HZB. XPS spectra were obtained by using non-monochromatized Al K_α (1486.58 eV) and Mg K_α (1253.56 eV) excitation from a SPECS XR 50 twin-anode X-ray source. The source and analyzer are arranged in “magic-angle” geometry (≈54.7° between X-ray propagation and analyzer axes). For the UPS measurements, He I (21.2 eV) and He II (40.8 eV) excitation from a Prevac UVS 40A2 gas-discharge lamp was used. In both cases the photoelectrons were detected by a ScientaOmicron Argus CU electron analyzer operating at a base pressure of <5 × 10^{–9} mbar. By setting the electron analyzer pass energy to 20 eV, total energy resolutions of 1.2 and 0.9 eV for excitation energies of Al K_α and Mg K_α, respectively, were achieved. The total energy resolution for the He I and He II UPS measurements was 100 meV. Binding energy calibration for XPS was carried by referencing the Au 4f_{7/2} peak to 84.00 eV; for UPS the Au Fermi

edge (E_F) was set to 0.00 eV. Samples were oriented with sample normal colinear with the analyzer entrance.

For fitting HAXPES and XPS spectra, Voigt functions were used to model individual spectral species; for a given photoemission line and experimental apparatus, the Gaussian and Lorentzian contributions were linked and optimized during simultaneous fitting of all measurements. Spin-orbit doublet separations were linked and optimized similarly, while doublet ratios were assigned based on the multiplicity of the core level. Furthermore, in cases where multiple contributions (i.e., from distinct chemical/electronic environments) to a photoemission line were present, the energy separation between contributions was linked and optimized during the fit procedure. This fit approach was intended to minimize the uncertainty in relative peak positions by constraining the fits to conform to a common physical model; the uncertainty in peak shifts was therefore primarily influenced by instability of the measurement apparatus, which was considered to be negligible compared to the more subjective errors in determining the VBM and CBM deriving spectral onsets of UPS and IPES spectra (discussed in detail below). The peak intensities were used to estimate stoichiometry of the measured samples according to the procedures described in the Supporting Information; relevant values are contained in (Table S1, Supporting Information).

The IPES measurements were performed in the same system as the lab-based XPS and UPS studies. A Kimball Physics inc. EGPS-1022E electron gun with a BaO cathode firing unit was used for excitation, and an OmniVac IPES1000 solid-state detector was used to record photon intensity. The base pressure during measurements was $<5 \times 10^{-9}$ mbar. The energy was calibrated by setting the Au E_F to 0.00 eV. The total energy resolution of this solid-state IPES setup is ≈ 1 eV.

Since both UPS and IPES are very surface sensitive techniques that can easily be affected by surface contaminations, a gentle cleaning procedure using subsequent Ar^+ ion treatment cycles with ion energies of 50 eV (i.e., energies significantly below any sputter threshold) was performed on the samples. To make sure that surface contaminations were being efficiently removed, Ar^+ ion treatment cycles of 20–30 min duration were performed with subsequent XPS measurements monitoring changes in C 1s (and for the CdS/CIGSe and CIGSe sample also the O 1s) spectra intensity. The Ar^+ ion treatment cycles were stopped when changes of the C 1s (O 1s) spectrum were no longer visible. For the bare CIGSe absorber this was the case after an accumulated Ar^+ ion treatment time of 120 min; for the absorbers with deposited buffer layers, i.e., CdS and GaO_x , an Ar^+ ion treatment of 200 min was needed. Exemplarily, the XPS survey spectra before and after 120 min Ar^+ treatment are shown for the bare CIGSe and the GaO_x /CIGSe sample in Figure S1 (Supporting Information).

The positions of the valence band maximum (VBM) and conduction band minimum (CBM) were derived by linear approximation of the leading edges of the UPS and IPES spectra, respectively. This inherently caused some uncertainty, in particular for the significantly less energy resolved IPES data. In this case, in an attempt to obtain the highest possible degree of accuracy, the determination of the relative changes of the IPES onsets were focused—and thence the CBOs. The following steps were performed: 1) A linear background obtained by a least-squares fit of the region below the calibrated E_F position (i.e., where no

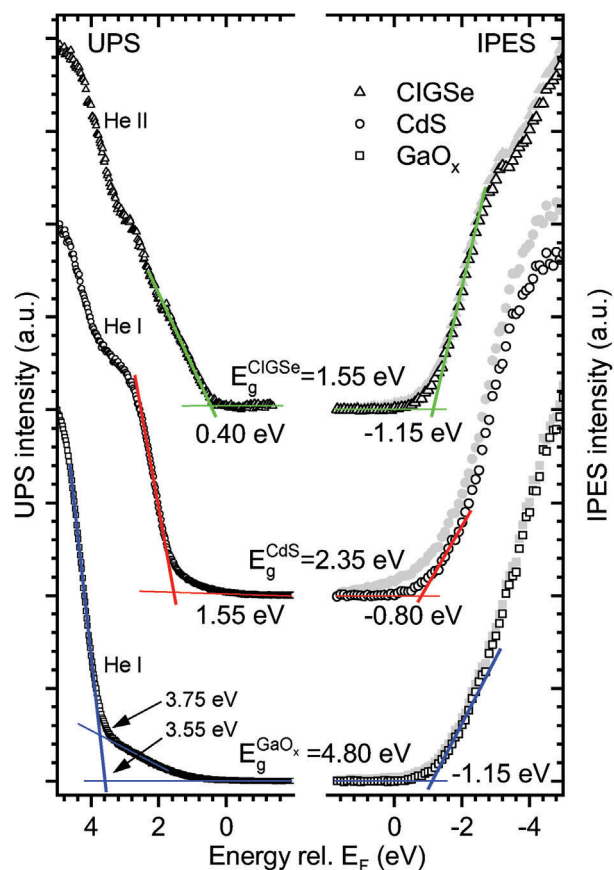


Figure 1. UPS (He I or He II excitation as indicated) and IPES spectra of the studied samples: bare CIGSe absorber (after 120 min of mild Ar^+ ion treatment) and CIGSe with nominal 50-nm-thick CdS and GaO_x buffer layer (after 200 min of mild Ar^+ ion treatment), respectively. The linear extrapolation of the leading edge positions of the UPS (± 0.10 eV for the bare CIGSe and the CdS/CIGSe sample and ± 0.15 eV for the GaO_x /CIGSe sample in absolute position) and IPES (± 0.20 eV in absolute position) spectra (and the computed surface band gap obtained from their differences (± 0.22 eV for the bare CIGSe and the CdS/CIGSe sample and ± 0.25 eV for the GaO_x /CIGSe sample)) are indicated. The IPES spectra have had a linear background subtracted; the background was obtained by a fit of the 0–2 eV region. The spectra before subtraction are plotted in light gray. Vertical offsets are added for clarity.

unoccupied states are possible) was subtracted from all spectra; the spectra before subtraction are shown in light-gray points in Figure 1. 2) The spectra were shifted and scaled such that their leading edges overlap over the largest possible energy range (see Figure S2, Supporting Information), and a common linear extrapolation (also shown in Figure S2, Supporting Information) was used to determine the intersection of the spectral leading edge with the background. This method attempted to eliminate the variations in the somewhat subjective process of determining the spectral leading edge—any suggested change to the line position would need to be applied to all spectra equally, leading to a uniform change in the absolute value of the obtained onsets with no change in their relative values. It is due to this argumentation that values derived from relative positions were assigned—i.e., the CBOs—with relatively low experimental uncertainty.

3. Results and Discussion

The HAXPES survey spectrum (see Figure S3, Supporting Information) of the bare CIGSe sample shows all expected peaks related to Cu, In, Ga, and Se. These CIGSe-related peaks are completely attenuated in the survey spectra of the samples with thick (nominally 50 nm) CdS and GaO_x buffer layers; and only respective buffer-related signals are observed, indicating complete coverage of the CIGSe by both CdS and GaO_x layers, with a buffer thickness exceeding the HAXPES information depth, which in this case is estimated to be between 20 and 30 nm.^[21]

Additional signals related to Na, O, and C can be identified in the survey spectrum of the bare CIGSe sample. The presence of Na at the CIGSe surface has repeatedly been observed before^[22–24] and is ascribed to thermally induced Na diffusion from the SLG through (and accumulation on top of) the CIGSe during absorber growth at elevated temperatures. The presence of O and C can be explained by surface contamination caused by the short exposure to air during sample mounting and introduction into the load lock of the HAXPES setup and/or incorporation of O and C into the CIGSe during absorber preparation. To some extent Na, O, and C signals can also be observed in the survey spectrum of the CdS/CIGSe sample, which can be explained by the same reasoning and thus points to a Na diffusion also into the CdS buffer. However, neither Na nor C is observed in the HAXPES survey spectrum of the GaO_x/CIGSe sample, suggesting that GaO_x prevents/reduces Na diffusion and that the C observed in the spectra of the (CdS)/CIGSe samples does indicate a (partial) incorporation into the buffer and absorber.

In this work, we use HAXPES data to derive the surface composition of the studied samples, as it is less affected by surface effects. Based on the shallow core levels Ga 3d, In 4d, and Cu 3p (see Figures S4, S5, Table S1, Supporting Information), we derived the CGI = [Cu]/([Ga]+[In]) and GGI = [Ga]/([Ga]+[In]) ratios for the bare CIGSe absorber surface to be 0.6 and 0.4 (±0.1), respectively (for a detailed description of the HAXPES data quantification see description in conjunction with Table S1, Supporting Information). Hence, the CIGSe surface is significantly Cu deficient compared to its expected bulk composition, in agreement with previous reports.^[25–27] As one explanation for this finding the formation of an OVC with Cu:(In+Ga):Se compositions of 1:3:5 or 1:5:8 at the CIGSe surface has been suggested in the past.^[8,9,28]

Next, the composition of the buffer layers is addressed. For the nominal 50-nm-thick CBD CdS buffer, the [Cd]/[S] ratio was derived based on the Cd 4d and S 2p measurements. To determine the GaO_x composition, we used the O 1s and the Ga 3d core levels of the nominal 50-nm-thick GaO_x buffer. As these photoemission lines have significantly different binding energies, the respective line intensities (derived by corresponding fits, see Figure S4 and S5, Supporting Information) had to be corrected by the corresponding photoionization cross-sections, the inelastic mean free paths (IMFP) of the photoelectrons, and the transmission function of the analyzer (for details see discussion in conjunction with Table S1, Supporting Information). For the CdS buffer, we find a slightly Cd-rich [Cd]/[S] ratio of 1.1 (±0.1); in agreement (within the experimental uncertainty) with the expected bulk composition ratio.^[18] For the GaO_x, we derive x to be 1.1 (±0.1), which matches well with the oxygen-deficient

(compared to stoichiometric Ga₂O₃) composition previously reported for amorphous GaO_x layers deposited in Ar₂ atmosphere (via pulsed laser deposition)^[29] or via oxidation of metallic Ga in 1 × 10⁻⁶ mbar partial pressure of O₂.^[30]

The UPS and IPES spectra of the CIGSe absorber with and without nominal 50-nm-thick CdS and GaO_x buffers, respectively, are plotted in Figure 1 on a common energy scale relative to the E_F level. The leading edge of the UPS and IPES spectra were obtained by linear extrapolation as discussed in the experimental section; they represent the VBM and CBM positions with respect to E_F, respectively. As the VBM (CBM) is usually below (above) E_F, the UPS leading edge = -VBM (IPES leading edge = -CBM), by convention. The UPS spectra were obtained using different excitation energies, i.e., He I (21.2 eV) for the CdS and GaO_x buffered samples, and He II (40.8 eV) for the bare CIGSe samples. The latter was specifically done to increase the photoionization cross section of the Cu 3d derived states that dominate the CIGSe VBM, outweighing the intensity decrease when going from He I to He II excitation.

While the extrapolation of the leading VB edges is relatively straightforward in the case of CIGSe (as the leading edge is formed by hybridized Se 4p—Cu 3d derived states^[31,32]) and CdS (as the leading edge is formed by S 3s—S 3p derived states^[31]), it is more complicated in the case of GaO_x. The dominating VB feature leading to the sloping onset at ≈ 4 eV is assigned to hybridized O 2p—Ga 4s derived states;^[3] however, there is significant spectral intensity visible between this edge and E_F, which has previously been ascribed to defect states related to oxygen vacancies.^[33,34] A contribution from band tails related to the amorphous structure of the deposited GaO_x is also likely. Hence, we will treat these states as being distinct from the “true” valence band and use the dominant O 2p—Ga 4s derived edge to determine the VBM. Figure 1 shows two intersections of the leading UPS edge with linear extrapolations of different backgrounds. In case (i), the above-edge defect states are treated as the background signal resulting in an onset position of 3.75 eV. This procedure approximates the leading edge that would result from subtraction of the defect-related states and linear extrapolation of the remainder. In case (ii), we extrapolate the main edge to the spectral noise floor observed around E_F, ignoring these states completely and resulting in a leading UPS edge position of 3.55 eV. This uncertainty dominates the error in deriving the VBM position of the GaO_x; thus, in Table 1 and associated calculations, we use the average of these two boundary values: (3.65 ± 0.15) eV. Together with the derived CBM position ((1.15 ± 0.20) eV), this results in a GaO_x surface band gap (E_g^{Surf} = CBM-VBM) of (4.8 ± 0.30) eV. This agrees well with the optically derived bulk band gap of 4.71 eV reported for similarly prepared GaO_x thin films.^[18] The VBM (±0.10 eV), CBM (±0.20 eV), and E_g^{Surf} (±0.25 eV) values for the bare CIGSe absorber (the 50-nm-thick CdS/CIGSe sample) are -0.40 (-1.55), 1.15 (0.80), and 1.55 (2.35) eV, respectively, as depicted in Figure 1. The values are in line with previous UPS/IPES measurements for CIGSe absorbers having similar surface CGI and GGI ratios (resulting in E_g^{Surf} values between 1.40 and 1.61 eV^[25–27]) and for CdS buffers (for which E_g^{Surf} values between 2.40 and 2.65 eV have been reported^[25,26]), in particular when considering the experimental uncertainty. As previously observed, the Cu-deficient CIGSe surface has a wider band gap (E_g^{Surf} = (1.55 ± 0.25) eV) than the absorber bulk.^[19,35]

Table 1. Core level binding energies (uncertainty $\approx \pm 0.02$ eV) and UPS/IPES leading edge (-VBM/-CBM) positions (see main text for uncertainties) used to calculate VBO and CBO at the CdS/CIGSe (top table) and GaO_x/CIGSe (bottom table) interfaces.

CdS/CIGSe interface	(bare ref.) CIGSe	(thick ref.) CdS/CIGSe	(thin) CdS/CIGSe	BE shift (thin – ref.)
In 4d _{5/2} (Mg K _α)	18.04 eV	–	18.17 eV	0.13 eV
Se 3d _{5/2} (Mg K _α)	54.36 eV	–	54.50 eV	0.14 eV
S 2p _{3/2} (Mg K _α)	–	161.92 eV	161.86 eV	–0.06 eV
Cd 3d _{3/2} (Mg K _α)	–	412.42 eV	412.41 eV	–0.01 eV
UPS leading edge	0.40 eV	1.55 eV	–	–
IPES leading edge	–1.15 eV	–0.80 eV	–	–
E _g ^{Surf}	1.55 eV	2.35 eV	–	–
VBO	–	–	–0.98 eV	–
CBO	–	–	–0.18 eV	–
GaO _x /CIGSe interface	(bare ref.) CIGSe	(thick ref.) GaO _x /CIGSe	(thin) GaO _x /CIGSe	BE shift (thin – ref.)
In 4d _{5/2} (6 keV)	17.72 eV	–	17.84 eV	0.12 eV
Se 3d _{5/2} (6 keV)	54.16 eV	–	54.26 eV	0.10 eV
Ga 3d _{5/2} (6 keV)	–	20.62 eV	20.69 eV	0.07 eV
UPS leading edge	0.40 eV	3.65 eV	–	–
IPES leading edge	–1.15 eV	–1.15 eV	–	–
E _g ^{Surf}	1.55 eV	4.80 eV	–	–
VBO	–	–	–3.21 eV	–
CBO	–	–	0.04 eV	–

To determine the VBO and CBO at the buffer/CIGSe interface, Kraut’s method is applied to determine the alignment at the intact interface.^[36] In this context, a sample with the “thinnest possible” closed buffer layer that is assumed to well-represent the interface in the regular layer stack and a surface-sensitive photoemission measurement are needed in order to isolate the core level binding energies at the interface (required to determine the interface-induced band bending) without “diluting” this information by integrating into the bulk of the sample.^[37–39] Unfortunately, for the GaO_x/CIGSe sample set it was not possible to obtain (closed) capping GaO_x layers thin enough to allow probing of the covered CIGSe absorber by surface-sensitive photoemission measurements. In this case, the interface could only be accessed by using HAXPES on samples with intermediate (nominally 5 nm) capping layer thicknesses; therefore, the contribution from the interface would be small, and any shift derived from these measurements should be considered a lower bound. The information is therefore considered to be incomplete, and we therefore increase the error budget of the derived energy level alignment in this case.

In both cases (CdS/CIGSe with XPS and GaO_x/CIGSe with HAXPES), we detect a shift of the In 4d and Se 3d peaks relative to the respective line positions at the surface of the bare (i.e., uncovered) CIGSe absorber. (NB: Unlike the measurement of the capping layer, the largest contribution of the buried CIGSe layer to the measured photoemission signal will originate from near the interface. However, when using bulk-sensitive HAXPES, the larger IMFP still means that the interface contribution is smaller, compared to when probed by more surface sensitive XPS measurements). The values needed to determine VBO and

CBO via Kraut’s method are depicted in Table 1 (a more detailed description of the methodology and data are found in SI, section “Derivation of the valence (VBO) and conducting (CBO) band offsets” including Figures S4–S7, Supporting Information). For the purpose of determining peak positions and shifts representing similar sample regions with high confidence, peaks with relatively low natural line widths and similar binding energies were selected.

By combining the UPS and IPES leading edge positions with the derived core-level shift values at the interface, the band offsets can be calculated according to the following equations:

$$VBO = (UPS_a + shift_a) - (UPS_b + shift_b) \quad (1)$$

$$CBO = (IPES_a + shift_a) - (IPES_b + shift_b) \quad (2)$$

where “a” and “b” denote the absorber and buffer, respectively. For shift_a and shift_b the average of the derived respective values for each core level was used. The resulting energy alignment for the CdS/CIGSe interface is shown in Figure 2a) and for the GaO_x/CIGSe interface, it is depicted in Figure 2b). The values for the VBM and CBM positions in the figures are corrected for the interface induced band bending. The CBOs between the CIGSe absorber and the buffer layers are crucial, because they govern the transport (and thus collection) of the electrons photogenerated in the absorber into the emitter. At the CdS/CIGSe interface, the formation of a “cliff-like” (i.e., negative) offset of (-0.18 ± 0.15) eV is derived. This is in contrast to the aligned^[10,11] or slightly positive^[11,12] CBO values reported for CdS/chalcopyrite stacks resulting in high-efficiency solar cells.

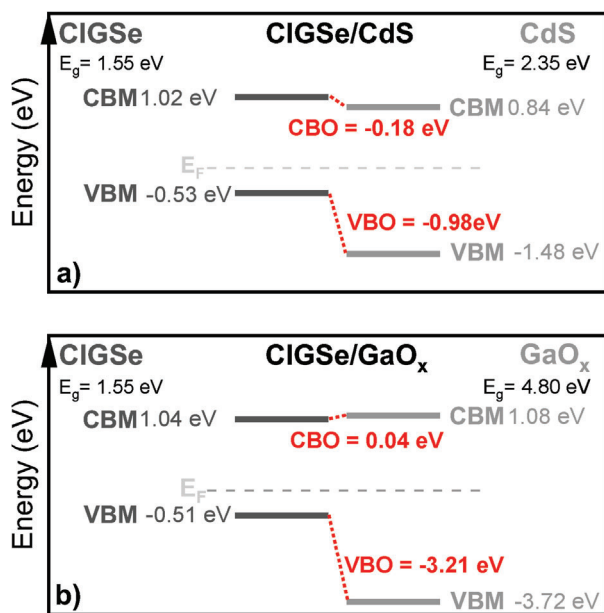


Figure 2. Energy level alignment at the interface between the CIGSe absorber layer and a) the CdS and b) the GaO_x buffer layer. Each stated value of VBM and CBM is corrected for interface-induced band bending effects. Please see text for the experimental uncertainties of the derived VBO and CBO values.

If a Cu-poor CIGSe surface layer is present, a negative CBO between -0.1 and -0.4 eV (depending on how in the underlying models the offset is distributed between the CdS/OVC and the OVC/CIGSe interfaces) would be in agreement with reaching high efficiencies.^[5-7] Thus, our finding might represent an interesting borderline case with respect to whether the derived CBO already limits the device efficiency. However, a conclusion on whether in the here studied case we have a rather small CBO at the OVC/CIGSe interface, which would mean that (for a high-efficiency devices) the acceptable “cliff-like” buffer/absorber CBO is rather small (i.e., -0.1 eV⁷) or whether the OVC/CIGSe CBO is similar to that at the CdS/OVC interface and thus the acceptable “cliff-like” CBO can be as large as -0.4 eV⁶ is not possible.

Subject to the caveats regarding the uncertainty in the core level binding energy shifts derived from the HAXPES measurements described above, for the GaO_x/CIGSe interface, we find nearly perfect alignment, with a small “spike-like” (i.e., positive) CBO of (0.04 ± 0.07) eV, which is in agreement with a buffer/absorber interface that principally could reach high efficiencies.^[5-7]

At both buffer/absorber interfaces, we find pronounced negative VB offsets ((-0.98 ± 0.15) eV for the CdS/CIGSe and (-3.21 ± 0.19) eV for the GaO_x/CIGSe interface) that are principally sufficient to block photo-generated holes preventing a high-rate recombination path across the buffer/CIGSe interface. However, despite having the seemingly better energy level alignment, solar cells with GaO_x buffer are clearly inferior to their counterparts with standard CdS buffer.^[18] This indicates that the spectral intensity above the VBM of GaO_x (see Figure 1) can indeed be ascribed to defect states that act as charge carrier recombination

centers, undermining the principally (almost) ideal electronic interface properties.

4. Conclusion

We directly measured VBM and CBM values, as well as core level shifts, for CdS/CIGSe GaO_x/CIGSe interfaces. While for the CdS/CIGSe interface a “cliff-like” CBO (-0.18 ± 0.07 eV) is found, for the GaO_x/CIGSe interface a small “spike-like” offset of (0.04 ± 0.07) eV is derived, which is seemingly the more ideal electronic interface structure in view of potentially reaching high solar cell efficiencies. However, this was found to be in contradiction to device results,^[18] showing that devices with standard CdS buffers outperform their counterparts with GaO_x buffer. This was tentatively being explained by the presence of significant density of occupied states above the GaO_x VBM, extending almost to E_F . These states (ascribed to band tails or to oxygen vacancy related defects) present in the significantly oxygen deficient amorphous GaO_x, with $x = 1.1 (\pm 0.1)$ derived by HAXPES, likely serve as charge carrier recombination centers in the working device and may account for the observed reduced open circuit voltage (V_{OC}) in the respective solar cells compared to CdS/CIGSe reference devices.

Supporting Information

Supporting Information is available from the Wiley Online Library or from the author.

Acknowledgements

Open access funding enabled and organized by Projekt DEAL.

Conflict of Interest

The authors declare no conflict of interest.

Data Availability Statement

The data that support the findings of this study are available in the supplementary material of this article.

Keywords

CdS buffer, chalcopyrite thin-film solar cell, energy level alignment, GaO_x buffer, interface properties

Received: December 30, 2023
Revised: February 21, 2024
Published online: March 8, 2024

- [1] M. Nakamura, K. Yamaguchi, Y. Kimoto, Y. Yasaki, T. Kato, H. Sugimoto, *IEEE J. Photovoltaics* **2019**, *6*, 1863.
- [2] M. A. Green, E. D. Dunlop, M. Yoshita, N. Kopidakis, K. Bothe, G. Siefert, X. Hao, *Prog. Photovolt.* **2023**, *31*, 651.

- [3] M. D. Heinemann, M. F. A. M. van Hest, M. Contreras, J. D. Perkins, A. Zakutayev, C. A. Kaufmann, T. Unold, D. S. Ginley, J. J. Berry, *Phys. Status Solidi A* **2017**, 214, 1600870.
- [4] T. Minemoto, Y. Hasimoto, Shams-Kolahi W., T. Satoh, T. Negami, H. Takakura, Y. Hamakawa, *Sol. Energy Mater. Sol. Cells* **2003**, 75, 121.
- [5] T. Minemoto, T. Matsui, H. Takakura, Y. Hamakawa, T. Negami, Y. Hashimoto, T. Uenoyama, M. Kitagawa, *Sol. Energy Mater. Sol. Cells* **2001**, 67, 83.
- [6] X. Liu, J. R. Sites, *AIP Conf. Proc.* **1996**, 353, 444.
- [7] F. Obereigner, N. Barreau, W. Witte, R. Scheer, *J. Appl. Phys.* **2015**, 117, 155704.
- [8] J. R. Tuttle, D. S. Albin, R. Noufi, *Solar Cells* **1991**, 30, 21.
- [9] D. Schmid, M. Ruckh, F. Grunwald, H. W. Schock, *J. Appl. Phys.* **1993**, 73, 2902.
- [10] M. Morkel, L. Weinhardt, B. Lohmüller, C. Heske, E. Umbach, W. Riedl, S. Zweigart, F. Karg, *Appl. Phys. Lett.* **2001**, 79, 4482.
- [11] S. Teshima, H. Kashiwabara, K. Masamoto, K. Kikunaga, K. Takeshita, T. Okuda, K. Sakurai, S. Ishizuka, A. Yamada, K. Matsubara, S. Niki, *MRS Online Proceedings Library* **2007**, 1012, 319.
- [12] S. Ishizuka, J. Nishinaga, K. Beppu, T. Maeda, F. Aoyagi, T. Wada, A. Yamada, J. Chantana, T. Nishimura, T. Minemoto, M. M. Islam, T. Sakurai, N. Terada, *Phys. Chem. Chem. Phys.* **2022**, 3, 1262.
- [13] F. Zang, H. Li, Y. T. Cui, G. L. Li, Q. Guo, *AIP Adv.* **2018**, 8, 045112.
- [14] S. Garud, N. Gampa, T. G. Allen, R. Kotipalli, D. Flandre, M. Batuk, J. Hadermann, M. Meuris, J. Poortmans, A. Smets, B. Vermang, *Phys. Status Solidi A* **2018**, 215, 1700826.
- [15] M. D. Heinemann, J. Berry, G. Teeter, T. Unold, D. Ginley, *Appl. Phys. Lett.* **2016**, 108, 022107.
- [16] S. I. Stepanov, V. I. Nikolaev, V. E. Bougrov, A. E. Romanov, *Adv. Mater. Sci.* **2016**, 44, 63.
- [17] J. Kim, T. Sekiya, N. Miyokawa, N. Watanabe, K. Kimoto, K. Ide, Y. Toda, S. Ueda, N. Ohashi, H. Hiramatsu, H. Hosono, T. Kamiya, *NPG Asia Mater.* **2017**, 9, e359.
- [18] H. A. Yetkin, T. Kodalle, T. Bertram, Villanueva Tovar A., R. Klenk, M. Rusu, J. Ibaceta-Jaña, F. Ruske, I. Simsek, R. Muydinov, B. Szyszka, R. Schlattmann, C. A. Kaufmann, *IEEE J. Photovolt.* **2021**, 11, 648.
- [19] M. D. Heinemann, R. Mainz, F. Österle, H. Rodriguez-Alvarez, D. Greiner, C. A. Kaufmann, T. Unold, *Sci. Rep.* **2017**, 7, 45463.
- [20] S. Ueda, Y. Katsuya, M. Tanaka, H. Yoshikawa, Y. Yamashita, S. Ishimaru, K. Kobayashi, *AIP Conf. Proc.* **2010**, 1234, 403.
- [21] QUASES-IMFP-TPP2M Ver. 3.0, Inelastic electron mean free paths calculated from the TPP-2M formula based on S. Tanuma, C. J. Powell, D. R. Penn, *Surf. Interf. Anal.* **1994**, 21, 165.
- [22] M. D. Heinemann, D. Greiner, T. Unold, R. Klenk, H. W. Schock, R. Schlattmann, C. A. Kaufmann, *IEEE J. Photovolt.* **2014**, 5, 378.
- [23] S. Puttnins, S. Levenco, K. Schwarzburg, G. Benndorf, F. Daume, A. Rahm, A. Braun, M. Grundmann, *Sol. Energy Mater. Sol. Cells* **2013**, 119, 281.
- [24] E. S. Mungan, X. Wang, M. A. Alam, *IEEE J. Photovolt.* **2012**, 3, 451.
- [25] K. Horsley, S. Pookpanratana, S. Krause, T. Hofmann, M. Blum, L. Weinhardt, M. Bär, K. George, J. Van Duren, D. Jackrel, C. Heske, presented at 37th IEEE Photovoltaic Specialists Conf., Seattle, WA, USA, June, **2011**.
- [26] N. Terada, R. T. Widodo, K. Itoh, S.-H. Kong, H. Kashiwabara, T. Okuda, K. Obara, S. Niki, K. Sakurai, A. Yamada, S. Ishizuka, *Thin Solid Films* **2005**, 480–481, 183.
- [27] E. Handick, P. Reinhard, J. H. Alsmeyer, L. Köhler, F. Pianezzi, S. Krause, M. Gorgoi, E. Ikenaga, N. Koch, R. G. Wilks, S. Buecheler, A. N. Tiwari, M. Bär, *ACS Appl. Mater. Interfaces* **2015**, 7, 27414.
- [28] H. Mönig, C. H. Fischer, R. Caballero, C. A. Kaufmann, N. Allsop, M. Gorgoi, R. Klenk, H. W. Schock, S. Lehmann, Lux-Steiner M. C., I. Lauerermann, *Acta Mater.* **2009**, 57, 3645.
- [29] L. Nagarajan, R. A. De Souza, D. Samuelis, I. Valov, A. Börger, J. Janek, K. D. Becker, P. C. Schmidt, M. Martin, *Nat. Mater.* **2008**, 7, 391.
- [30] T. E. Hsieh, J. Frisch, R. G. Wilks, M. Bär, *ACS Appl. Mater. Interfaces* **2023**, 15, 47725.
- [31] T. V. Kuznetsova, V. I. Grebennikov, H. Zhao, C. Derks, C. Taubitz, M. Neumann, C. Persson, M. V. Kuznetsov, I. V. Bodnar, R. W. Martin, M. V. Yakushev, *Appl. Phys. Lett.* **2012**, 101, 111607.
- [32] S. Siebentritt, M. Igalson, C. Persson, S. Lany, *Prog. Photovolt.* **2010**, 18, 390.
- [33] L. Dong, R. Jia, B. Xin, B. Peng, Y. Zhang, *Sci. Rep.* **2017**, 7, 40160.
- [34] Z. Hajnal, J. Miró, G. Kiss, F. Réti, P. Deák, R. C. Herndon, J. M. Kuperberg, *J. Appl. Phys.* **1999**, 86, 3792.
- [35] C. Rincón, R. Márquez, *J. Phys. Chem. Solids* **1999**, 60, 1865.
- [36] E. A. Kraut, R. W. Grant, J. R. Waldrop, S. P. Kowalczyk, *Phys. Rev. Lett.* **1980**, 44, 1620.
- [37] D. Wippler, R. G. Wilks, B. E. Pieters, van Albada S. J., D. Gerlach, J. Hüpkes, M. Bär, U. Rau, *ACS Appl. Mater. Interfaces* **2016**, 8, 17685.
- [38] O. Romanyuk, A. Paszuk, I. Bartoš, R. G. Wilks, M. Nandy, J. Bombsch, C. Hartmann, R. Félix, S. Ueda, I. Gordeev, J. Houdkova, P. Kleinschmidt, P. Machek, M. Bär, P. Jiříček, T. Hannappel, *Appl. Surf. Sci.* **2021**, 565, 150514.
- [39] O. Romanyuk, O. Supplie, A. Paszuk, J. P. Stoeckmann, R. G. Wilks, J. Bombsch, C. Hartman, Garcia-Diez R., S. Ueda, I. Bartoš, I. Gordeev, J. Houdkova, P. Kleinschmidt, M. Bär, *Surf. Interface Anal.* **2020**, 52, 933.